AIAA JOURNAL
Vol. 48, No. 1, January 2010

Simulation of Supersonic Combustion Involving H_2/Air and C_2H_4/Air

P. G. Keistler* and H. A. Hassan†
North Carolina State University, Raleigh, North Carolina 27695-7910

DOI: 10.2514/1.43213

A turbulence model that calculates the turbulent Prandtl and Schmidt numbers as part of the solution is presented. This model also accounts for compressibility effects, and addresses turbulence/chemistry interaction. Its predictions are compared with two experiments: an axisymmetric case involving mixing, hydrogen combustion, and ethylene combustion; and a three-dimensional ethylene mixing experiment. Fair to good agreement is indicated in the cases where data is available. Chemical mechanisms are found to have an influence on autoignition for hydrogen combustion cases, and on ignition location and flame size for hydrogen/ethylene combustion cases using reduced mechanisms.

Nomenclature

C	=	model constants
D	=	diffusion coefficient
h	=	enthalpy
k	=	turbulent kinetic energy
P	=	pressure
Pr	=	Prandtl number
Sc	=	Schmidt number
s	=	stoichometric oxidizer/fuel mass ratio
u_i	=	velocity vector
Y	=	mass fraction
y^+	=	dimensionless wall distance
Z	=	mixture fraction
α	=	diffusivity
β	=	model constants
$\Delta h_{f,m}$	=	heat of formation of species m
ε	=	dissipation rate
ζ	=	enstrophy
ν	=	kinematic viscosity
ρ	=	density
σ	=	variance of concentrations
τ	=	time scale
$\dot{\omega}$	=	production rate

Subscripts

f	=	fuel
h	=	enthalpy
m	=	species
o	=	oxidizer
t	=	turbulent
Y	=	mass fraction

Superscripts

$''$	=	fluctuation
$\tilde{}$	=	Favre average
$\bar{}$	=	time average

Presented as Paper 0028 at the 47th AIAA Aerospace Sciences Meeting, Orlando, FL, 5–8 January 2009; received 13 January 2009; accepted for publication 21 September 2009.

*Graduate Student, Mechanical and Aerospace Engineering Department. Student Member AIAA.

†Professor, Mechanical and Aerospace Engineering Department. Fellow AIAA.

Introduction

SIMULATION of turbulent combustion in scramjet engines requires highly sophisticated models in order to address the complex flow physics involved. Typical turbulence models only consider velocity fluctuations, but earlier work [1] has shown that specification of the turbulent Prandtl number Pr_t and turbulent Schmidt number Sc_t have a profound influence on the simulation. In high-speed reacting flows, concentrations and temperature fluctuations are as important as velocity fluctuations, and must be included in the model. In order to assess the impact of these fluctuations, equations for the variance of enthalpy and its dissipation rate, as well as the variance of concentrations and its dissipation rate are required. These equations, which provide the turbulent thermal diffusivity and diffusion coefficients, are derived from the exact compressible Navier–Stokes equations and modeled term by term in the same way the k-ζ turbulence model was developed [2].

Compressibility is another important aspect of supersonic mixing in that it limits the spreading rate of injected fuel. The model of [3] is used, which has been previously validated with three sets of supersonic mixing experiments [4–6]. It has been suggested in [7] that three-dimensional effects may result in enhanced spreading rate of simple shear layers for certain range of convective Mach numbers. Data compiled by Settles and Dodson [8] showed that there is a great deal of scatter in measured spreading rates of compressible shear layers. This cast doubt on the validity of the correlation derived in [7] and its general applicability to complex shear flows.

Turbulence/chemistry interaction is also an important part of supersonic combustion. Traditionally, assumed or evolution probability density functions (PDFs) are used to address this. It was shown in [9] that calculations using assumed and evolution PDFs produced comparable mean flows, but the assumed PDF was unable to predict higher-order correlations, such as those involving chemical source terms, with any accuracy. Also, evolution PDFs require a large amount of storage and computational time, since they require Monte Carlo simulation. Because of these restrictions, the terms involving chemical production rates were modeled as in [10].

The chemical kinetic model also plays an important role in supersonic combustion. Differences among chemical models can affect the ignition location or the temperature at which a simulation will autoignite. Four distinct chemical models are considered here, two for vitiated air/hydrogen combustion [11,12], and two reduced chemical models for vitiated air/ethylene combustion [13,14].

Predictions of this model, which includes all of the above aspects, are compared with the experiments of the Office of the Secretary of Defense's Test Media Effects Program (OSD-TME) [15]. The

purpose of this program is to examine the effects of the differences between ground tests and flight tests of supersonic combustors, in particular the use of vitiated air in place of regular air and its effects on flame holding and other aspects related to chemical kinetics [16,17]. Also, a particular experiment of Lin et al. [18] involving normal injection of ethylene into a cold Mach 2 flow is considered.

Formulation of the Problem

Governing Equations

The variable Pr_t and Sc_t formulations employed in this work are based on equations for the variance of enthalpy and its dissipation rate and variance of concentrations and its dissipation rate. The need for such a formulation is a result of the fact that low values of Sc_t can enhance mass transfer and subsequent heat release to such an extent that they may result in unstarts. On the other hand, high values of Sc_t will result in the restriction of turbulent mass transfer to values that could not sustain combustion. Similarly, reduced values of Pr_t result in increased thermal diffusion away from the flame holding, which could result in a flame blowout.

In order to allow for variable Pr_t and variable Sc_t, expressions for the turbulent thermal diffusivity and the turbulent diffusion coefficient must be derived. The most logical way to achieve this goal is to employ a procedure similar to that in deriving the eddy viscosity. Thus the variance equations are similar to the turbulent kinetic energy equation, while the rates of dissipation of the variances are similar to the length scale equation which, in this work, is the enstrophy equation.

The variance of enthalpy $\tilde{h}''^2$ and its dissipation rate ε_h provide an expression for α_t, the turbulent diffusivity in the form

$$\alpha_t = 0.5(C_h k \tau_h + \nu_t/\beta_h) \tag{1}$$

where

$$\tau_h = \tilde{h}''^2/\varepsilon_h, \qquad \varepsilon_h = \overline{\alpha\left(\frac{\partial h''}{\partial x_i}\right)^2} \tag{2}$$

ν_t is the turbulent eddy viscosity,

$$\nu_t = C_\mu k^2/\nu\zeta, \qquad C_\mu = 0.09 \tag{3}$$

$C_h = 0.0648$ and $\beta_h = 0.5$ are model constants, α is the laminar diffusivity, ν is the molecular kinematic viscosity, k is the turbulent kinetic energy per unit mass or variance of velocity, and ζ is the enstrophy or variance of vorticity. Similarly, the variance of concentrations σ_Y

$$\sigma_Y = \sum \tilde{Y}_m''^2 \tag{4}$$

where Y_m'' is the fluctuation of the mass fraction of species m, and its dissipation rate, ε_Y,

$$\varepsilon_Y = \sum \overline{D\left(\frac{\partial Y_m''}{\partial x_i}\right)^2} \tag{5}$$

yield the turbulent diffusion coefficient D_t as

$$D_t = 0.5(C_Y k \tau_Y + \nu_t/\beta_Y) \tag{6}$$

where

$$\tau_Y = \sigma_Y/\varepsilon_Y \tag{7}$$

$C_Y = 0.065$ and $\beta_Y = 0.5$ are model constants, and D is the molecular binary diffusion coefficient. Both C_Y and C_h were obtained from Launder [19]. Moreover, β_h and/or β_Y are chosen so as to produce the desired constant turbulent Prandtl and/or Schmidt number if such numbers are constant. The choice of α_t and D_t is a result of the experiments of Abe et al. [20] in simple shear flows. It is indicated there that the approximate time scale for temperature fluctuation is proportional to the average of τ_h and τ_k. A similar expression is used for D_t.

The equation for σ_Y, the variance of concentrations, contains the term

$$\sum \overline{Y_m''\dot{\omega}_m}$$

where $\dot{\omega}_m$ is the production rate of species m. Similarly, the equation that governs the enthalpy variance contains the term

$$\sum \overline{h''\dot{\omega}_m \Delta h_{f,m}}$$

where $\Delta h_{f,m}$ is the heat of formation of species m. Traditionally, the above terms are evaluated by using assumed or evolution PDFs, or ignored completely. Because such terms are important, a modeling approach was implemented in [10]. Thus,

$$2\sum \overline{Y_m''\dot{\omega}_m} = C_{Y,8} \sum \sqrt{\tilde{Y}_m''^2}\,\overline{\dot{\omega}_m} \tag{8}$$

and

$$\sum \overline{h''\dot{\omega}_m \Delta h_{f,m}} = C_{h,12}\sqrt{\tilde{h}''^2} \sum \overline{\dot{\omega}_m \Delta h_{f,m}} \tag{9}$$

where $C_{Y,8} = 0.4$ and $C_{h,12} = 0.86$ are model constants, and $\overline{\dot{\omega}_m}$ is the value of $\dot{\omega}_m$ using mean temperature and mass fractions. Because evolution PDF methods are computationally intensive requiring extensive computer time and excessive storage, the above modeling results in a highly efficient algorithm.

The compressibility correction results from the dilatational dissipation term $4/3[\nu\overline{\rho(u_{i,i}'')^2}]$ and a pressure work term $\bar{u}_i''(\partial P/\partial x_i)$ that appear in the k equation. As indicated earlier, compressibility effects severely restrict the spreading rate of free shear layers at high Mach numbers and thus have a profound influence on mixing and combustion. The variety of models given in [21] assume the dilatational dissipation term to be proportional to $M_t \sim k/a^2$, the turbulent Mach number. In the k-ζ model the term is modeled as [2]

$$\frac{4}{3}\nu\overline{\rho(u_{i,i}'')^2} = C_1\bar{\rho}k/\tau_\rho, \qquad C_1 = 0.6 \tag{10}$$

where

$$\frac{1}{\tau_\rho} = \frac{1}{\bar{\rho}}\left[k\left(\frac{\partial\bar{\rho}}{\partial x_i}\right)^2\right]^{\frac{1}{2}} \tag{11}$$

The pressure work term is modeled as

$$\bar{u}_i''\frac{\partial P}{\partial x_i} = \frac{\nu_t}{C_k\bar{\rho}}\frac{\partial\bar{\rho}}{\partial x_i}\frac{\partial P}{\partial x_i} \tag{12}$$

The turbulent Prandtl number Pr_t and the turbulent Schmidt number Sc_t are given by

$$\mathrm{Pr}_t = \frac{\nu_t}{\alpha_t} \quad \text{and} \quad \mathrm{Sc}_t = \frac{\nu_t}{D_t} \tag{13}$$

These numbers do not enter directly in obtaining the solution but can be outputted at any time. The governing equations and model constants used in this investigation are given in [10].

Numerical Procedure

A modification of REACTMB [22], a code that has been under development at North Carolina State University for the last several years, is employed in this investigation. It is a general purpose parallel Navier–Stokes solver for multicomponent, multiphase reactive flows at all speeds. It solves the Favre averaged form of the Navier–Stokes equations. It employs a second order essentially nonoscillatory and/or total-variation-diminishing upwind method

based on the low-diffusion flux-splitting scheme of Edwards [23] to discretize the inviscid fluxes while central differences are employed for the viscous and diffusion terms. A planar Gauss–Seidel method is used for the implicit time advancement. The code is parallelized using domain decomposition and message passing strategies. Finite rate chemical kinetic models are used to address chemical non-equilibrium.

Since REACTMB uses multiple grid domains per processor, the grid is split into a large number of blocks in order to obtain a desirable load distribution. The code also uses a shared memory location for the implicit Jacobian of each block. Therefore, in large three-dimensional cases, the grid is split into a larger number of blocks in order to reduce the total memory requirements.

Boundary Conditions

A ghost cell method is used to impose boundary conditions. The temperature is specified by a constant value in the ghost cell. This allows the actual wall temperature to change in response to the local flow conditions, while still remaining close to a specified value. As for the turbulent quantities, k must be equal to zero at the wall, while ζ obeys the following condition:

$$\nu\zeta_w = \frac{\partial}{\partial n}\left(\nu\frac{\partial k}{\partial n}\right)\bigg|_w \tag{14}$$

This condition is obtained from the limiting form of the k equation in the near wall region. Similar procedures are employed in developing boundary conditions for the additional turbulent quantities introduced by the variable turbulent Schmidt and Prandtl number models.

Chemical Kinetic Models

Vitiated Air/H_2

Two completely distinct H_2/Air mechanisms are considered. The first is the seven species/seven reactions model developed by Jachimowski [11]. In this mechanism, the seven species considered are H_2, O_2, OH, H_2O, H, and O together with the inert species N_2. All reaction rates in this model are functions of temperature. The second is the nine species/nineteen reaction mechanism developed by Connaire et al. [12]. This model considers all of the above species as well as HO_2 and H_2O_2. Moreover, the reaction rates are both pressure and temperature dependent. This model was developed for combustion over a temperature range of 298–2700 K, a pressure range of 0.01–87 atmospheres and equivalence ratios from 0.2–6.

Vitiated Air/H_2/C_2H_4

Two sets of reduced kinetic models are employed for C_2H_4/Air combustion. The first is that of Gokulakrishnan et al. [13]. In this model, a one-step reaction $C_2H_4 + O_2$ resulting in C_2H_2O and H_2O is employed. This is followed by a detailed $C_2H_2O/H_2/O_2$ kinetic model that includes 14 species and 44 reactions. The second is that of Zambon and Chelliah [14], which employs the quasi-steady-state (QSS) approximation. The equations that result from QSS are, in general, nonlinear. The distinguishing feature of this approach is that the solution of the resulting algebraic equation is explicit, thus increasing efficiency. The resulting reduced model consists of 18 elementary reactions involving 22 species.

Results and Discussion

A schematic of the OSD-TME experiment is shown in Fig. 1. The center jet in this axisymmetric device consists of vitiated air at Mach 1.6. The test enthalpies ranged from that of Mach 5 to Mach 7 flight. The fuel is injected at low subsonic speeds through a coflow nozzle angled 30° toward the main jet. The Mach number for the injected fuel is approximately 0.2. This relatively low speed is required for safe operation. If the fuel were injected at or above Mach 1, and failed to ignite, the test chamber would fill with fuel quicker than it could be purged, producing a potentially dangerous situation. The pressure at the nozzle exit is atmospheric and total temperature in the coflow

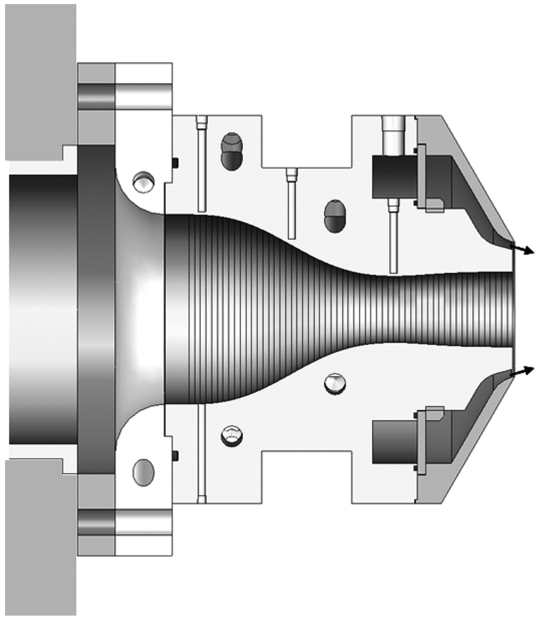

Fig. 1 Schematic of OSD-test media effects experiment (courtesy of A. D. Cutler) [14].

nozzle is near ambient. Experiments were conducted without coflow fuel, as well as with hydrogen alone, ethylene alone, and a hydrogen ethylene mix. The runs chosen for computations are listed in Table 1. In this table, phi is the equivalence ratio of the listed fuel. Note that there is no case with pure ethylene fuel. This is due to the fact that no steady combustion of ethylene alone was obtainable with the selected range of test enthalpies. The cases without coflow fuel will be referred to as the mixing cases. The block layout of the grid used for all of the OSD-TME experiments is shown in Fig. 2. The measurements in this experiment were taken using a dual pump CARS-IRS system for simultaneous measurements of temperature, species concentrations, and two velocity components [24–26]. The error associated with these experimental measurements is 50–100 K for the temperatures and 30–100 m/s for the velocities. The computational grid for the OSD-TME cases employs 74 blocks and contains 236,480 cells. The refined grid employs 122 blocks and contains 377,024 cells. Note that these grids make use of the axisymmetry of the experiment. The grid distribution is such that cells are clustered near walls and regions with strong gradients. The wall spacing is determined by requiring that the maximum y^+ value be less than 1.0. The grid refinement produced negligible change in the solution; therefore, the presented results are those obtained with the original grid.

A schematic of the ethylene injection experiment is shown in Fig. 3. The injector, which is normal to the main flow, is circular and has a diameter of 0.1875 in. The Mach 2 airstream has a static temperature and pressure of 300 K and 241,317 Pa, respectively. The ethylene injection nozzle has a stagnation temperature of 315 K and a stagnation pressure of 127,553 Pa. The main flow boundary layer thickness at the exit of the injector was about 0.24 in. The block layout of this three-dimensional case is shown in Fig. 4. Ethylene mixture fraction is measured at three streamwise planes using a Raman scattering technique [16]. The computational grid for this case employs 248 blocks and contains 3,768,320 cells.

Table 1 OSD—test media effects experiment conditions

Run number	Enthalpy	P0, Pa	T0, K	Phi H2	Phi C2H4
M27–M75	Mach 5.5	402,500	1218	——	——
M79–M95	Mach 5.5	429,400	1376	——	——
H57	Mach 5.5	414,400	1319	1	——
E40a	Mach 6	421,300	1523	0.7	——
E40b	Mach 6	421,300	1523	0.7	0.53

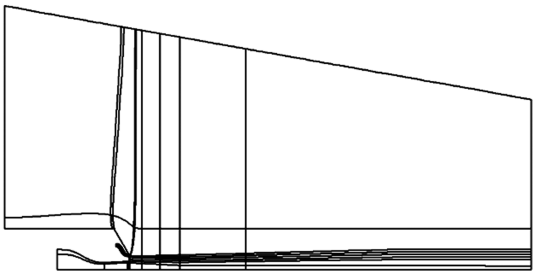

Fig. 2 Block layout for OSD-TME computations.

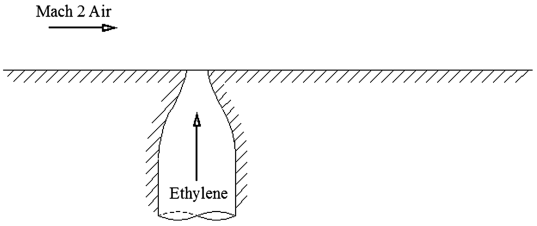

Fig. 3 Schematic of ethylene injection case.

Vitiated Air/Air

There are two sets of data for the mixing cases of the OSD-TME experiments, radial temperature profiles at various streamwise locations and axial velocity along the centerline and two radial locations of the nozzle. As can be seen in Table 1, the average stagnation temperature for the near field measurements, which were taken in runs M27–M75, is significantly lower than the average for the far field measurements, which were taken in runs M79–M95. The same trend is observed in the stagnation pressure. Simulations were carried out using both of these averages and are presented together with the experimental data.

Figures 5a and 5b show measured and computed temperature profiles for eight different streamwise locations. For the most part, there is good agreement. Note that there is some asymmetry in the experimental data. This is most likely due to a shifted reference point in the measurements, not an asymmetry in the jet itself. The experimental data is presented here unaltered. Also note the appearance of two different experimental profiles at the 40 cm station. This has been attributed to the fact that half of the measurements came from the higher average temperature runs. Figure 6 shows the 40 cm station by itself with error bars on the experimental values. The diamond symbols and line represent the "upstream" measurements, which were at a lower stagnation temperature, and the square symbols and line represent the "downstream" measurements, which were taken at a higher stagnation temperature. Predictions are within the standard deviation for all but three points. Figure 7 shows the measured and computed axial velocities along the centerline of the jet. The measured velocities are significantly higher than either of the computed profiles. The cause of this difference is unknown. Given the measured temperatures along the centerline, these velocities correspond to approximately Mach 1.8–1.9 flow. The nozzle is designed for

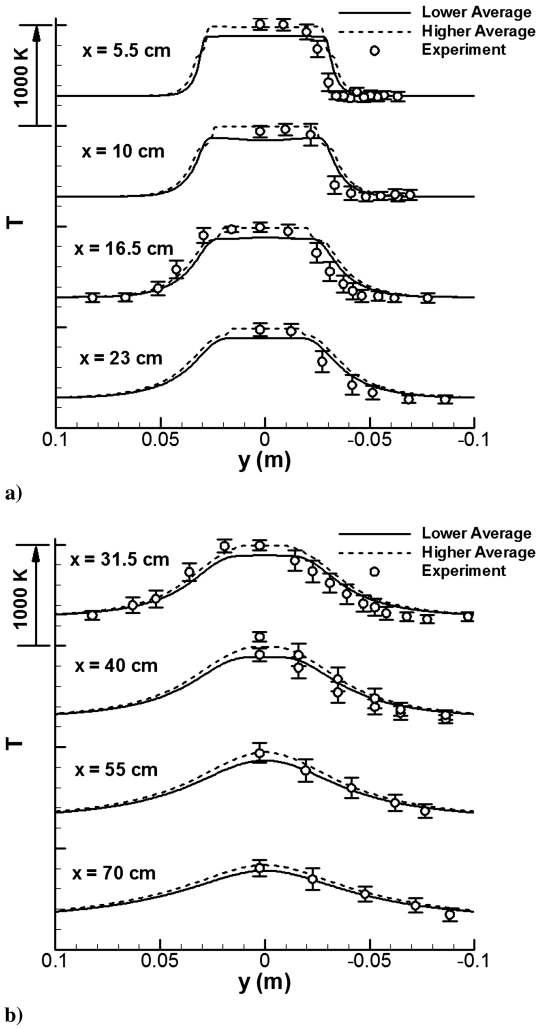

Fig. 5 Radial temperature profiles for OSD-TME mixing runs.

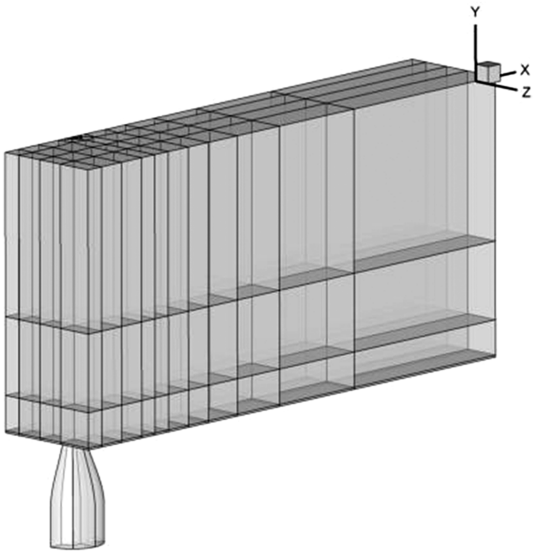

Fig. 4 Block layout for ethylene injection case.

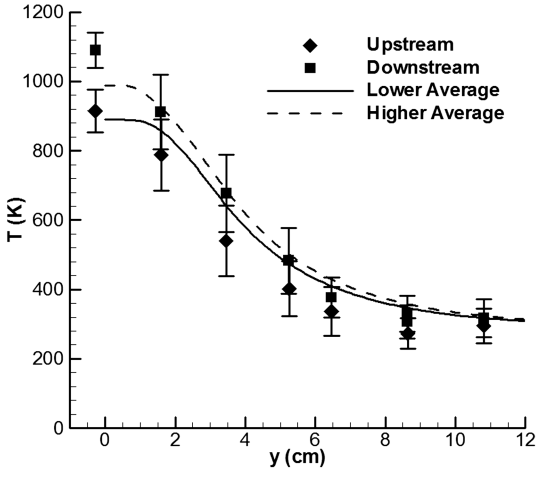

Fig. 6 Radial temperature profiles at 40 cm station.

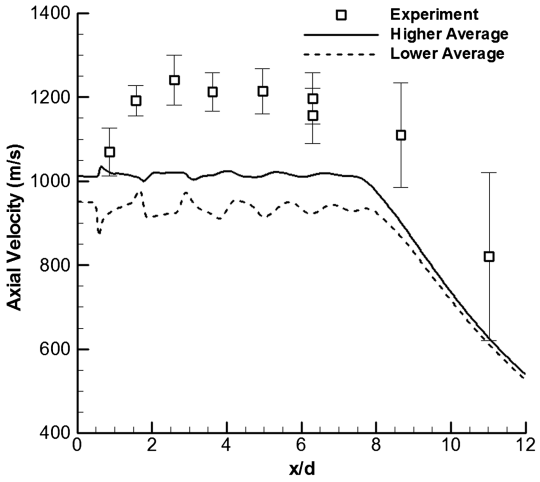

Fig. 7 Axial velocity along centerline for OSD-TME mixing runs.

Mach 1.6 operation, which both of the simulations predict. Radial velocity profiles at $x/d = 2.6$ and $x/d = 11$ are shown in Figs. 8a and 8b. These locations correspond to the 16.5 cm and 70 cm stations. There is a similar discrepancy between the computed and experimental data here, as expected. However, the computed profiles are consistent with those from VULCAN, as shown in [23]. The appearance of noise in the experimental data for $x/d = 11$ is due to the fact that each point, other than the centerline point, is the average of only two simultaneous measurements. Finally, the computed

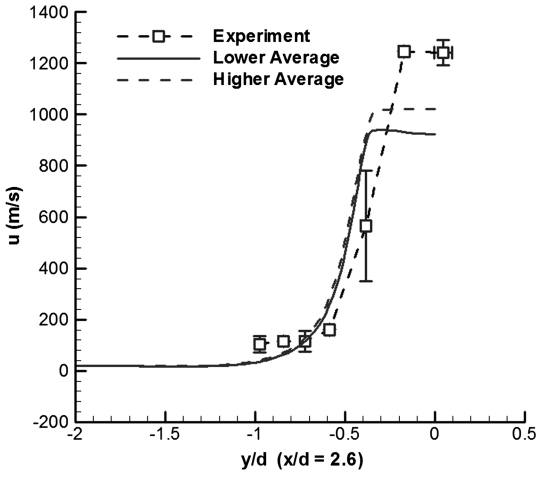

a)

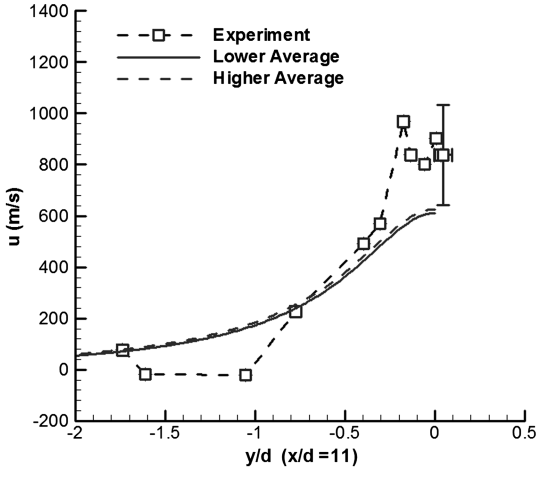

b)

Fig. 8 Axial velocity along radial profile for OSD-TME mixing runs.

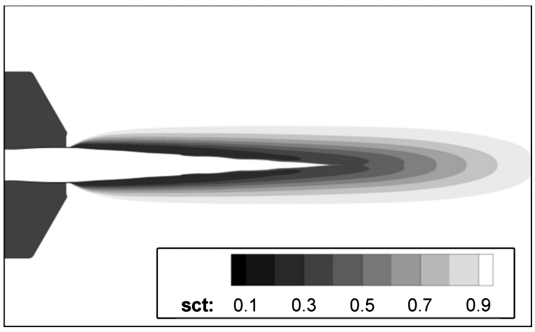

Fig. 9 Computed turbulent Schmidt number contours for OSD-TME mixing runs.

turbulent Schmidt number contour is shown in Fig. 9. Note the variation from the specified floor value of 0.2 to 1.0 across the mixing region of the jet.

Vitiated Air/Air/H_2

While there is no quantitative experimental data for run H57 of the OSD-TME experiment, an infrared image is included for qualitative comparison. This image can be seen in Fig. 10. The hydrogen is injected at atmospheric pressure and temperature with a mass flow rate corresponding to an equivalence ratio of 1.0. The purpose of these computational runs is to compare the two chemical models. Figure 11 shows the computed H_2O mole fractions for each of the chemical models, with Jachimowski on the top half and Connaire on the bottom half. Note that while the solutions are similar, the Connaire model is much less likely to autoignite. In this case, it was restarted from an ignited Jachimowski run, at which point it sustained the combustion and produced similar results to those of the Jachimwoski mechanism. Figures 12 and 13 show contours of

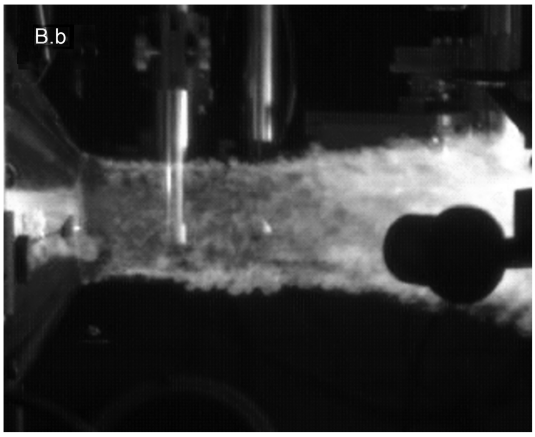

Fig. 10 Infrared image of run H57.

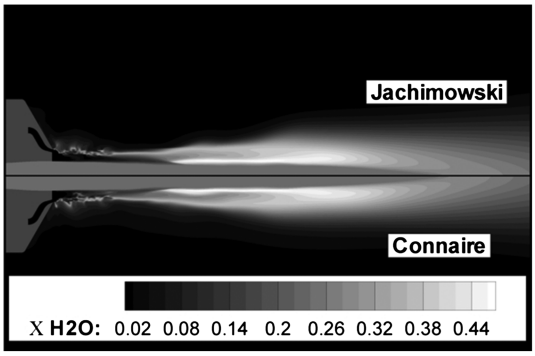

Fig. 11 Computed H_2O mole fraction contours for OSD-TME run H57.

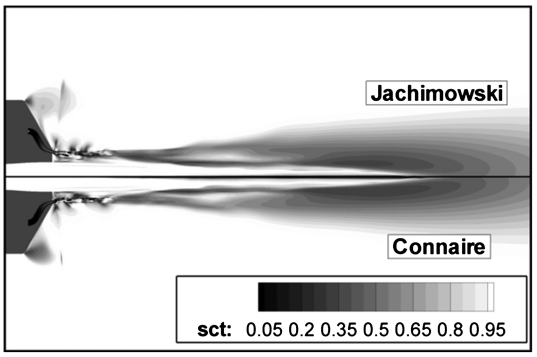

Fig. 12 Computed turbulent Schmidt number contours for OSD-TME run H57.

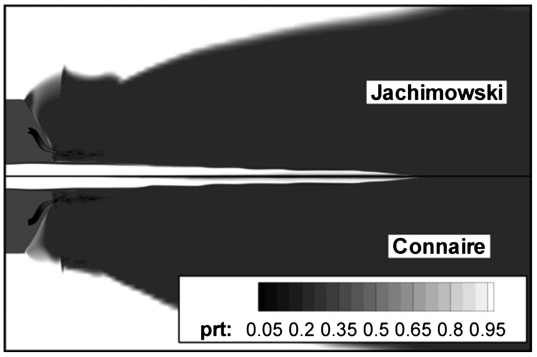

Fig. 13 Computed turbulent Prandtl number contours for OSD-TME run H57.

turbulent Schmidt number and turbulent Prandtl number, respectively.

An additional run was performed using the Jachimowski mechanism on a refined grid, which doubled the number of cells in the streamwise direction. The ignition location and the overall solution remained unchanged.

Vitiated Air/Air/C_2H_4

The first case involving ethylene is the normal injection mixing experiment. Contours of air density on the symmetry plane are shown in Fig. 14. This figure is included to show the structure of the flow, and to indicate the locations of the measurement planes. These planes are located at 5, 10, and 25.3 diameters down stream of the jet. Figure 15 shows the contours of ethylene mixture fraction on these three planes, measured quantities on the left and computed quantities on the right. Mixture fraction is defined by the following formula.

$$Z = (sY_f - Y_o + Y_{o,o})/(s + Y_{o,o}) \tag{15}$$

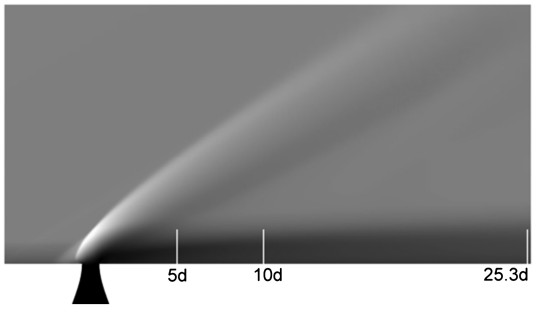

Fig. 14 Computed symmetry plane air density contours for ethylene injection experiment.

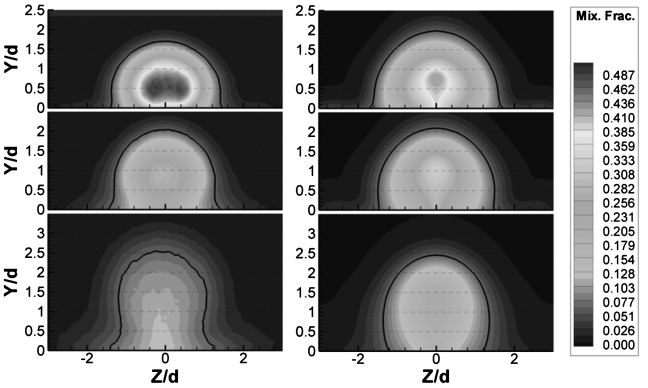

Fig. 15 Measured (left) and computed (right) mixture fraction contours for ethylene injection experiment.

where

$$s = (X_o M_o)/(X_f M_f) \text{ at stoichometric} \tag{16}$$

The subscript o denotes oxidizer and f denotes fuel. In this case, these correspond to oxygen and ethylene. $Y_{o,o}$ represents the mass fraction of oxidizer in the air stream. In Eq. (15), X and M represent mole fraction and molecular weight, respectively. There is fair agreement between computation and experiment here. The first station predicts a lower concentration of fuel in the center of the jet, while the third station shows a higher concentration than experiment. The black line on the plots represents the stoichometric line. Finally the computed turbulent Schmidt number contours are shown in Fig. 16.

The second case involving ethylene is run E40 of the OSD-TME experiments. This run is split into two phases, E40a and E40b. During the first phase, the coflow contains only hydrogen, with a target equivalence ratio of 0.5. During the second phase, which is initiated after steady combustion is achieved in the first phase, the coflow fuel contains both hydrogen and ethylene, each with a target equivalence ratio of 0.5. The actual equivalence ratios for this particular run can be seen in Table 1. The target enthalpy is that of Mach 6 flow. Again, no quantitative experimental data is available. A visible image of each phase is shown in Fig. 17. This case was used as a comparison of the two reduced ethylene mechanisms described above, the 15-species model of Gakulakrishnan et al. [13] and the 22-species model of Zambon and Chelliah [14]. Figure 18 shows the H_2O contours for run E40a, where only hydrogen is present in the coflow fuel. The 15 species model is on top and the 22 species model is on the bottom. The 22 species model predicts a much earlier ignition and an overall smaller flame. The same trend is observed for run 40b, which is shown in Fig. 19. The structure is essentially the

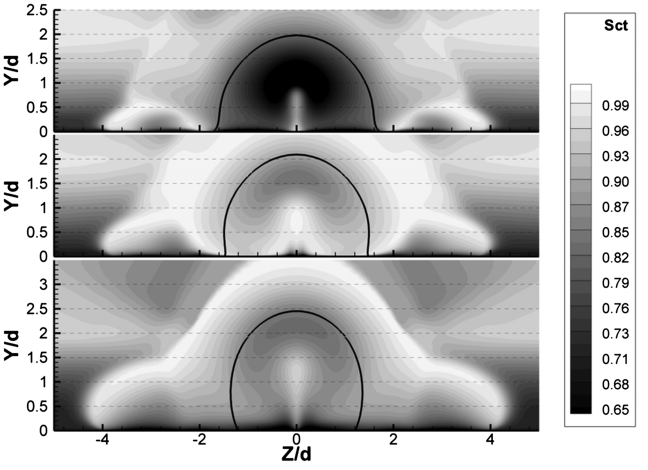

Fig. 16 Computed turbulent Schmidt number contours for ethylene injection experiment.

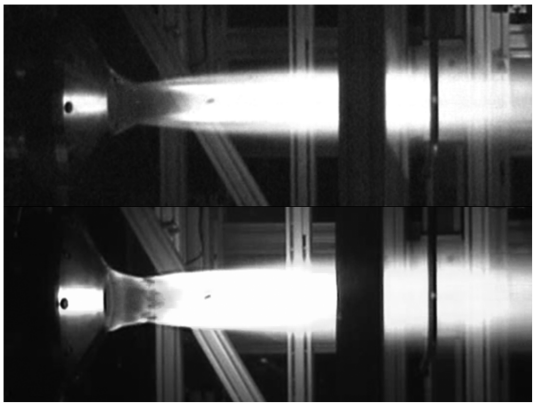

Fig. 17 Visible images of OSD-TME experiment, runs E40a (top) and E40b (bottom).

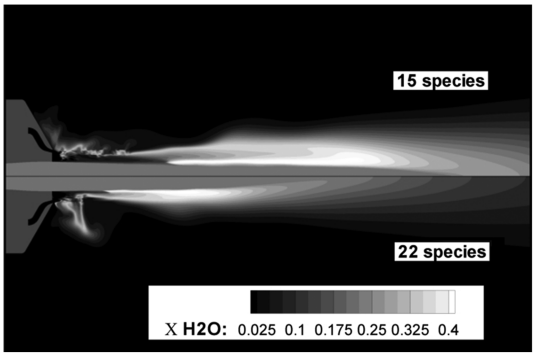

Fig. 18 Computed H_2O mole fraction contours for OSD-TME experiment, run 40a.

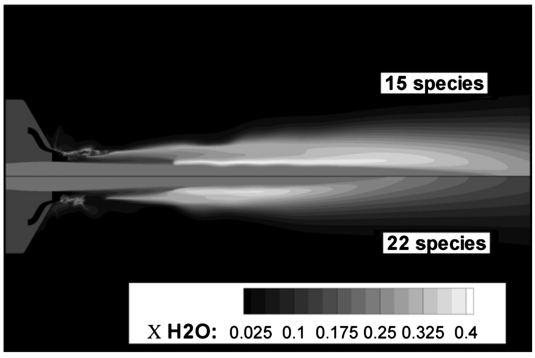

Fig. 19 Computed H_2O mole fraction contours for OSD-TME experiment, run 40b.

same, but for the 22 species model the ignition location moves slightly downstream when the ethylene is introduced. Referring back to visible images in Fig. 17, this slight movement is to be expected.

Conclusions

A comprehensive turbulence model is presented that calculates the turbulent Prandtl and Schmidt numbers as part of the solution. This model also models the turbulence/chemistry interaction and accounts for compressibility effects.

Two sets of experiments are examined in this study. The first is an axisymmetric annular jet under a variety of conditions: a case with no coflow, a case with hydrogen fuel, and a case with a mixture of hydrogen and ethylene fuel. The second is a three-dimensional case where ethylene is allowed to mix with cold air. Fair to good agreement is indicated in all cases, but some cases were only compared qualitatively in the absence of experimental data.

The role of chemical kinetic mechanism is determined to have an impact on autoignition for the hydrogen-only cases, and a signification impact on ignition location and flame size for hydrogen/ethylene mixtures. Because of the absence of quantitative experimental measurements, it is difficult to determine which ethylene reduced model is better.

All calculations are based on the model developed in [10]. Based on the above results, it is suggested that this model could be used as a basis for scramjet designs. Obviously, there is a need for nonintrusive experimental data for further validation of the model.

Acknowledgments

The authors would like to thank the Test Resource Management Center (TRMC) Test and Evaluation/Science and Technology (T&E/S&T) Program for their support. This work is funded by the T&E/S&T Program through the High-Speed/Hypersonic Test focus area managed by Arnold Engineering Development Center, Arnold Air Force Base, Tennessee.

References

[1] Baurle, R. A., and Eklund, D. R., "Analysis of Dual-Mode Hydrocarbon Scramjet Operation at Mach 4–6.5," *Journal of Propulsion and Power*, Vol. 18, No. 5, 2002, pp. 990–1002. doi:10.2514/2.6047

[2] Robinson, D. F., and Hassan, H. A., "Further Development of the k-ζ (Enstrophy) Turbulence Closure Model," *AIAA Journal*, Vol. 36, No. 10, 1998, pp. 1825–1833. doi:10.2514/2.298

[3] Alexopoulos, G. A., "A k-ζ (Enstrophy) Compressible Turbulence Model for Mixing Layers and Wall Bounded Flows," *AIAA Journal*, Vol. 35, No. 7, 1997, pp. 1221–1224. doi:10.2514/2.219

[4] Samimy, M., and Elliot, G. S., "Effect of Compressibility on Characteristics of Free Shear Layers," *AIAA Journal*, Vol. 28, No. 3, 1990, pp. 439–445. doi:10.2514/3.10412

[5] Elliot, G. S., and Samimy, M., "Compressible Effects in Free Shear Layers," *Physics of Fluids A*, Vol. 2, No. 7, 1990, pp. 1231–1240. doi:10.1063/1.857816

[6] Goebel, S. G., and Dutton, J. C., "Experimental Study of Compressible Turbulent Mixing Layers," *AIAA Journal*, Vol. 29, No. 4, 1991, pp. 538–546. doi:10.2514/3.10617

[7] Papamoschou, D., "Effect of Three-Dimensionality on Compressible Mixing," *Journal of Propulsion and Power*, Vol. 8, No. 1, 1992, pp. 247–249. doi:10.2514/3.23467

[8] Settles, G. S., and Dodson, L. J., "Hypersonic Turbulent Boundary Layer and Free Shear Database," NASA CR 177610, April 1993.

[9] Baurle, R. A., Hsu, A. T., and Hassan, H. A., "Assumed and Evolution Probability Density Functions in Supersonic Turbulent Combustion Calculations," *Journal of Propulsion and Power*, Vol. 11, No. 6, 1995, pp. 1132–1138. doi:10.2514/3.23951

[10] Xiao, X., Hassan, H. A., and Baurle, R. A., "Modeling Scramjet Flows with Variable Turbulent Prandtl and Schmidt Numbers," *AIAA Journal*, Vol. 45, No. 6, 2007, pp. 1415–1423. doi:10.2514/1.26382

[11] Jachimowski, C. J., "An Analytic Study of the Hydrogen-Air Reaction Mechanism with Application to Scramjet Combustion," NASA Technical Paper 2791, February 1988.

[12] Connaire, M. O., Curran, H. J., Simmie, J. M., Pitz, W. J., and Westbrook, C. K., "A Comprehensive Modeling Study of Hydrogen Oxidation," *International Journal of Chemical Kinetics*, Vol. 36, No. 11, 2004, pp. 603–622. doi:10.1002/kin.20036

[13] Gokulakrishnan, P., Pal, S., Klassen, M. S., Hamer, A. J., Roby, R. J., Kozaka, O., and Menon, S., "Supersonic Combustion Simulation of Cavity-Stabilized Hydrocarbon Flames Using Ethylene Reduced Kinetic Mechanism," AIAA Paper 2006-5092, July 2006.

[14] Zambon, A. C., and Chelliah, H. K., "Explicit Reduced Reaction Models for Ignition, Flame Propagation, and Extinction of $C_2H_4/CH_4/H_2$ and Air Systems," *Combustion and Flame*, Vol. 150, Nos. 1–2, 2007, pp. 71–91. doi:10.1016/j.combustflame.2007.03.003

[15] Drummond, J. P., Danehy, P. M., Bivolaru, D., Gaffney, R. L., Parker, P., Chelliah, H. K., Cutler, A. D., Givi, P., and Hassan, H. A., "Predicting the Effects of Test Media in Ground-Based Propulsion Testing," *2006 Annual ITEA Technology Review*, Cambridge, MA, 7–10 Aug. 2006.

[16] Cutler, A. D., Magnotti, G., Capriotti, D. P., and Mills, C. T., "Supersonic Combusting Jet Experiments for Code Development and Validation," *55th JANNAF Propulsion Meeting*, Boston, MA, 2008.

[17] Danehy, P. M., Magnotti, G., Bivolaru, D., Tedder, S., and Cutler, A. D., "Simultaneous Temperature and Velocity Measurements in a Large-Scale, Supersonic, Heated Jet," *55th JANNAF Propulsion Meeting*, Boston, MA, 2008.

[18] Lin, K., Ryan, M., Carter, C., Gruber, M., and Raffoul, C., "Scalability of Ethylene Gaseous Jets for Fueling Scramjet Combustors at Various Scales," AIAA Paper 2009-1423, Jan. 2009.

[19] Launder, B. E., "Heat and Mass Transport," *Turbulent Topics in Applied Physics*, edited by P. Bradshow, Vol. 12, Springer–Verlag, Berlin, 1978.

[20] Abe, K., Kondoh, T., and Nagano, Y., "A New Turbulence Model for Predicting Flow and Heat Transfer in Separating and Reattaching Flows-2. Thermal Field Calculations," *International Journal of Heat and Mass Transfer*, Vol. 38, No. 8, 1995, pp. 1467–1481. doi:10.1016/0017-9310(94)00252-Q

[21] Wilcox, D. C., *Turbulence Modeling for CFD*, 2nd ed., DCW Industries, Inc., La Cañada, CA 1998.

[22] Edwards, J. R., "Advanced Implicit Algorithm for Hydrogen-Air Combustion Calculation," AIAA Paper 1996-3129, June 1996.

[23] Edwards, J. R., "A Low Diffusion Flux Splitting Scheme for Navier–Stokes Calculation," *Computers and Fluids*, Vol. 26, No. 6, 1997, pp. 635–659. doi:10.1016/S0045-7930(97)00014-5

[24] Tedder, S., Bivolaru, D., Danehy, P. M., Weikl, M. C., Beyrau, F., Seeger, T., and Cutler, A. D., "Characterization of a Combined CARS and Interferometric Rayleigh Scattering System and Demonstration in a Mach 1.6 Combustion-Heated Jet," AIAA Paper 2007-0871, Jan. 2007.

[25] Tedder, S. A., Danehy, P. M., Magnotti, G., and Cutler, A. D., "CARS Temperature Measurements in a Combustion-Heated Mach 1.6 Jet," AIAA Paper 2009-0524, Jan. 2009.

[26] Bivolaru, D., Cutler, A. D., Danehy, P. M., Gaffney, R. L., Jr., and Baurle, R. A., "Spatially and Temporally Resolved Measurements of Velocity in a H2-Air Combustion-Heated Supersonic Jet," AIAA Paper 2009-0027, Jan. 2009.

J. Gore
Associate Editor